1 *Article*

2 Low-Loss Lithium Niobate on Insulator (LNOI)
3 Waveguides of a 10 cm-Length and
4 a Sub-Nanometer Surface Roughness

5 **Rongbo Wu** [1,2,†], **Min Wang** [3,4,†], **Jian Xu** [3,4], **Jia Qi** [1,2], **Wei Chu** [1,4], **Zhiwei Fang** [3,4],
6 **Jianhao Zhang** [1,2], **Junxia Zhou** [3,4], **Lingling Qiao** [1], **Zhifang Chai** [3,4], **Jintian Lin** [1],
7 **and Ya Cheng** [1,3,4,5,*]

8 [1] State Key Laboratory of High Field Laser Physics, Shanghai Institute of Optics and Fine Mechanics,
9   Chinese Academy of Sciences, Shanghai 201800, China; rbwu@siom.ac.cn (R.W.); qijia@siom.ac.cn
10   (J.Q.); chuwei0818@qq.com (W.C.); jhzhang@siom.ac.cn (J.Z.); qiaolingling@siom.ac.cn (L.Q.);
11   jintianlin@siom.ac.cn (J.L.)
12 [2] University of Chinese Academy of Sciences, Beijing 100049, China;
13 [3] State Key Laboratory of Precision Spectroscopy, East China Normal University, Shanghai 200062,
14   China; mwang@phy.ecnu.edu.cn (M.W.); jxu@phy.ecnu.edu.cn (J.X.); zwfang@phy.ecnu.edu.cn
15   (Z.F.); 1780497299@qq.com (J.Z.); zfchai@phy.ecnu.edu.cn (Z.C.)
16 [4] XXL—The Extreme Optoelectromechanics Laboratory, School of Physics and Materials Science, East
17   China Normal University, Shanghai 200241, China
18 [5] Collaborative Innovation Center of Extreme Optics, Shanxi University, Taiyuan, Shanxi 030006,
19   China
20
21 * Correspondence: ya.cheng@siom.ac.cn (Y.C.)
22 † These authors contributed equally to this paper.

23

24 **Abstract:** We develop a technique for realizing lithium niobate on insulator (LNOI)
25 waveguides of a multi-centimeter-length with a propagation loss as low as 0.027 dB/cm. Our
26 technique relies on patterning a chromium (Cr) thin film coated on the top surface of LNOI
27 into a hard mask with a femtosecond laser followed by the chemo-mechanical polishing for
28 structuring the LNOI into the waveguides. The surface roughness on the waveguides is
29 determined to be 0.452 nm with an atomic force microscope (AFM). The approach is
30 compatible with other surface patterning technologies such as optical and electron beam
31 lithographies or laser direct writing, enabling high-throughput manufacturing of large-scale
32 LNOI-based photonic integrated circuits.

33 **Keywords:** lithium niobate, waveguide, photonic integrated circuit, propagation loss, optical
34 lithography, chemo-mechanical polishing
35

36 1. Introduction

37   Photonic integrated circuits (PICs) have shown promising potential for realizing complex
38 information processing systems employing both quantum and classical light sources [1,2]. To
39 increase the computational efficiency and reconfigurability, the crucial requirements for the
40 PIC-based optical computers/calculators are low propagation loss, fast tunability, and efficient
41 optical interfacing. Currently, several materials have been utilized to construct large-scale PICs,
42 including silicon and some semiconductor materials [3-6], fused silica [7,8] and bulk lithium
43 niobate (LN) [9,10]. The advantage of silicon-based PICs is the high refractive index of silicon

44 which can allow for fabricating compact light circuits with strong confinement and tight bends.
45 In addition, the lithographic technology for high precision patterning of silicon and
46 semiconductors is mature. However, silicon-based PICs intrinsically suffer from a relatively
47 high propagation loss and a transmission window prohibitive for visible and shorter
48 wavelengths. PICs can be built on fused silica and bulk LN crystals by local modification of the
49 refractive index with either illumination of light or ion doping. Unfortunately, the refractive
50 index increases achieved using these approaches are usually on the orders of 10^{-3} to 10^{-2},
51 resulting in large footprints of the PICs as required for minimizing the bending loss. Most
52 importantly, the typical propagation losses of waveguides in the state-of-the-art PICs are
53 typically on the order of 10^{-1} dB/cm or higher, which sets an ultimate limitation on the
54 performance of the PIC-based optical computers.
55   Recently, a revolutionary approach for building high performance PICs has been
56 emerging enabled by the successful demonstration of high quality lithium niobate on insulator
57 (LNOI) nanophotonic structures. The first experimental proof of this approach is provided by
58 first patterning the LNOI into the designated geometries using a femtosecond laser. The draft
59 structures obtained after the femtosecond laser patterning, which has a relatively high sidewall
60 roughness on the order of tens of nanometers, are then polished with a focused ion beam (FIB)
61 milling to smoothen the sidewall [11]. This concept was soon extended to incorporate with
62 other lithographic technologies such as optical lithography and electron beam writing (EBW)
63 for defining the planar patterns on LNOI substrates followed by reactive ion etching to
64 complete the nanostructuring of the LNOI [12,13]. The initial focus was mainly placed on
65 optical microresonators [11-21], and other devices such as waveguides and photonic crystals
66 [22-28] appeared shortly, taking the advantage of high surface smoothness of the sidewalls as
67 a result of the ion dry etching. So far, the propagation loss in the LNOI waveguides has reached
68 0.04 dB/cm which opens the avenue toward large-scale PIC applications [29].
69   It is noteworthy that the ion etching step which is necessary for achieving the high quality
70 sidewalls on the LNOI nanophotonic structures inherently leaves a low but non-negligible
71 surface roughness which is difficult to be completely removed [29]. Moreover, the use of FIB
72 or EBW in the patterning of LNOI makes the approach impractical for fabricating large-scale
73 PICs owing to their low throughputs and limited ranges of motion. Recently, we have
74 developed a technique for fabricating high quality optical microresonators on LNOI with a
75 quality factor above 10^7 [30]. Since this technique does not involve any ion beam etching
76 processes, surface smoothness beyond that allowed by ion beam etching can be readily
77 achieved, and the footprint sizes of PICs can be greatly increased by patterning the LNOI
78 photonic structures with either laser direct writing or optical lithography. Here, we
79 experimentally show that we are able to realize 10 cm-long LNOI waveguides of a propagation
80 loss of 0.027 dB/cm which is benefited from the low surface roughness of 0.452 nm measured
81 with an atomic force microscope (AFM). The low loss waveguides can be essential building
82 blocks for light modulation, beam delivery and manipulation, nonlinear optics, and optical
83 signal processing.

84

2. Materials and Methods
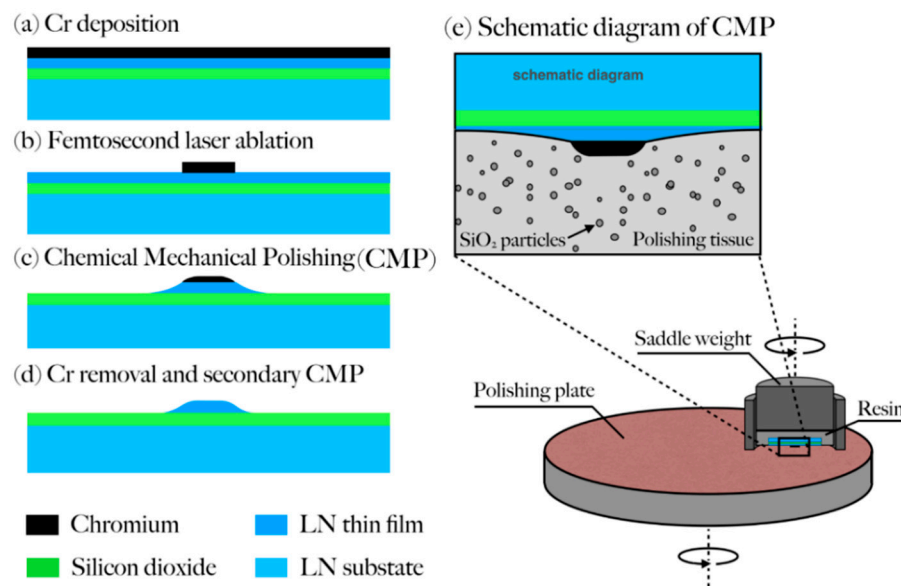
Figure 1. (**a**)-(**d**) Flow-chart of fabrication of lithium niobate on insulator (LNOI) waveguide and (**e**) schematic diagram of chemo-mechanical polishing (CMP).

In our experiment, the LNOI waveguides were produced on a commercially available X-cut LNOI wafer fabricated by ion slicing (NANOLN, Jinan Jingzheng Electronics Co., Ltd.) [31]. The LN thin film with a thickness of 400 nm is bonded to a 2 μm thick SiO_2 layer grown on a LN substrate. The fabrication process includes four steps, as schematically illustrated in Figure 1. First, a thin layer of chromium (Cr) with a thickness of 600 nm was deposited on the surface of the LNOI by magnetron sputtering. Subsequently, the patterning of Cr film on the LNOI sample was carried out using femtosecond laser ablation. Specifically, to minimize the heat effect as well as the redeposition of the ablation debris on the surface, the femtosecond laser ablation was conducted by focusing the femtosecond laser beam onto the top surface of LNOI sample which was immersed in water. The key in this step is to carefully choose a pulse energy of the femtosecond laser so as to enable a complete removal of the Cr film without damaging the underneath LNOI thanks to the high precision and low heat generation in the interaction of femtosecond laser pulses with various types of materials [32]. The detailed parameters of femtosecond laser ablation are provided as follows. We used a femtosecond laser with a center wavelength of 1030 nm, a pulse width of 170 fs, and a tunable repetition rate ranging from 2.5 kHz to 83.3 kHz (PHAROS, LIGHT CONVERSION) for the Cr film patterning. A variable neutral density filter was used for adjusting the average power. A 100× objective lens (M Plan Apo NIR, Mitutoyo Corporation) with a numerical aperture (NA) of 0.7 was used to produce a tightly focused spot of ~ 1 μm diameter. The LNOI sample was mounted on a computer-controlled XY motion stage (ABL15020WB and ABL15020, Aerotech) with a translation resolution of 100 nm, whereas positioning of the focus of laser beam in the Z direction was achieved with another one-dimensional motion stage of a translation resolution of 100 nm (ANT130-110-L-ZS, Aerotech) onto which the objective lens was mounted. A charged coupled device (CCD) connecting with the computer was installed above the objective lens to monitor the fabrication process in real time. The laser power was chosen to be 0.2 mW at which a complete removal of the Cr thin film can be realized, while the LNOI underneath the Cr film remains intact for its relatively higher damage threshold than Cr. The remaining Cr disk formed on the LNOI serves as a hard mask for the subsequent CM polishing.

The CM polishing process was conducted using a wafer polishing machine (NUIPOL802, Kejing, Inc.). In the CM polishing process, we used a piece of velvet polishing cloth, and the

119   polishing slurry (MasterMet, 60 nm amorphous colloidal silica suspension) was provided by
120   Buehler, Ltd. The soft velvet cloth allows not only the Cr film but also the exposed LNOI to be
121   accessed by the polishing slurry. Since the Cr film is of a higher hardness than that of the LNOI,
122   the exposed LNOI could be preferentially removed in the CM polishing process before the
123   sacrifice of the Cr mask. Moreover, by carefully controlling the duration of the CM polishing
124   process, the side wall angle with respect to the vertical direction of the fabricated LNOI
125   nanostructures can be controlled from a few degrees for a long polishing duration to nearly 80°
126   for a short duration of the polishing process. Finally, the fabricated structure was first
127   immersed in a Cr etching solution (Chromium etchant, Alfa Aesar GmbH) for 10 min to remove
128   the Cr mask, and then polished again at a relatively low polishing pressure with a shorter
129   polishing duration to improve the smoothness of the upper surface of LN waveguide.


130
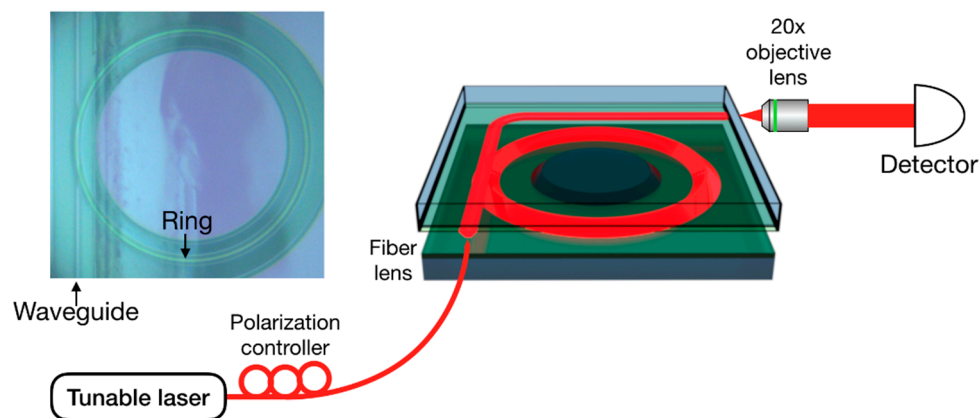
131   **Figure 2.** Schematic of the experimental setup for measuring the Q factor of the microring
132   resonator. Left inset: Optical micrograph image of the microring resonator coupling with the
133   waveguide, as indicated by the black arrows.

134   To characterize the propagation loss in the LNOI waveguide, we constructed a whispering
135   gallery ring resonator by which the propagation loss of the LNOI waveguide can be determined
136   using $\alpha = 2\pi n_{eff} / (Q\lambda)$, where α is the attenuation coefficient, n_{eff} the effective refractive index,
137   Q the quality factor of the ring resonator, and λ the wavelength of the light beam. Both the n_{eff}
138   and the Q-factor can be determined from the transmission spectrum of microring resonator.
139   The experimental setup for measuring the Q factor of the ring resonator is schematically shown
140   in Figure 2. The light produced by a tunable laser (LTB-6728, New Focus) was coupled into a
141   curved LNOI waveguide whose geometric parameters including the thickness and width are
142   the same as that of the LNOI ring by use of a fiber lens. The exiting light was collected by a 20×
143   objective lens (MPlanFL N, OLYMPUS) into a detector (Model 1811, New Focus). The bend of
144   the upper waveguide was intentionally introduced for preventing the stray light from the fiber
145   laser from entering the objective lens located in front of the detector. The polarization direction
146   of the light was adjusted with a fiber polarization controller. The curved waveguide was
147   coupled to the LNOI ring resonator by evanescent coupling. Specifically, by carefully adjusting
148   the distance between the coupling waveguide and the microring resonator, we are able to
149   achieve the critical coupling condition which is crucial for obtaining an accurate intrinsic Q
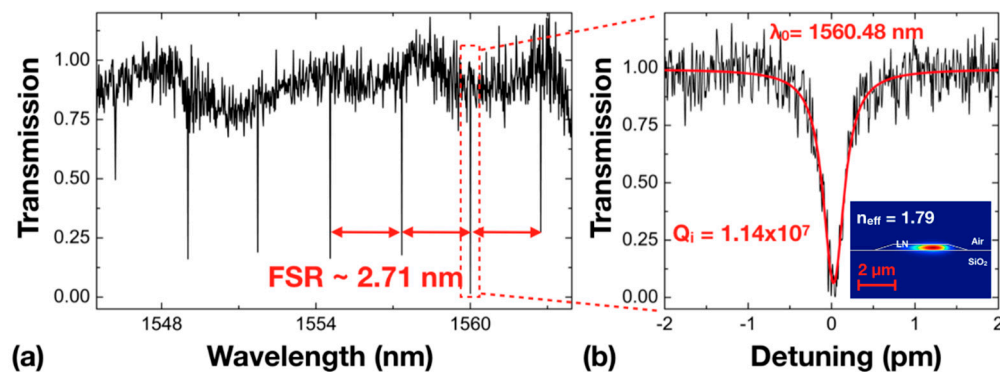150   factor of the ring resonator.

151

152   **3. Results**

153
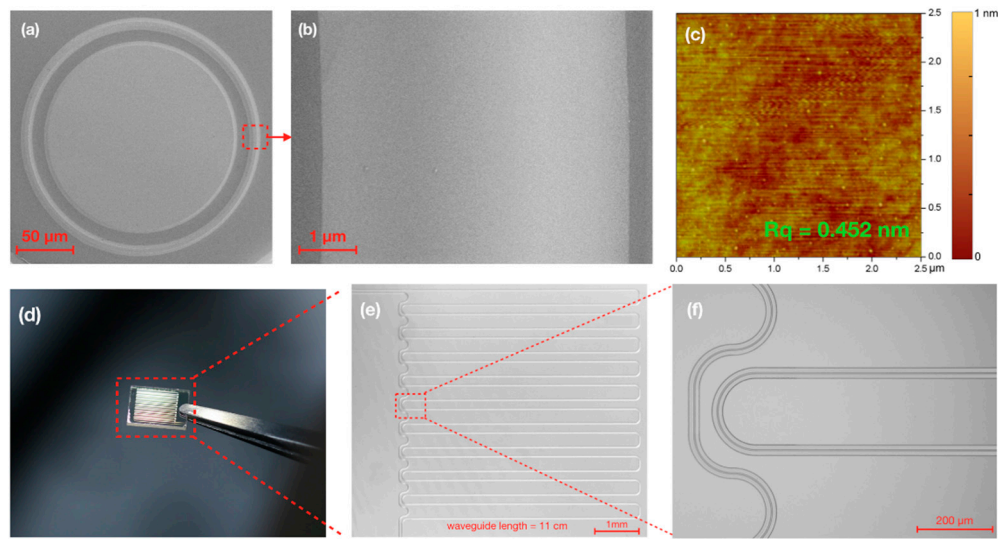
154   **Figure 3.** (**a**) Top-view scanning electron microscope (SEM) image of a LN microring resonator.
155   (**b**) Zoomed view of the ridge of the microring resonator in (a). (**c**) Atomic force microscope
156   (AFM) image of the ridge. (**d**) Picture of a chip consisting of an 11 cm-long waveguide captured
157   by digital camera. (**e**)-(**f**) Zoomed images of the waveguides on the chip captured by an optical
158   microscope.

159   Figure 3a shows the top-view scanning electron microscope (SEM) images of a LN micro
160   ring resonator with a diameter of 160 μm and the width of the waveguide is ~3 μm. The close-
161   up-view SEM of an arc of the ring highlights the high surface smoothness on the CM polished
162   sample. A further atomic force microscope (AFM) inspection as illustrated in Figure 3c
163   confirms that a surface roughness as low as R_q= 0.452 nm has been achieved. The same
164   fabrication technique was also used to fabricate a continuous 11 cm-long optical waveguide as
165   shown by the digital-camera-captured picture in Figure 3d, with the details being given by the
166   zoomed optical micrographs in Figure 3e - f. The total time of femtosecond laser ablation for
167   fabricating the 11 cm-long waveguide is 90 min. At this moment, the footprint size of the PICs
168   is only limited by the LNOI wafer size. Technically speaking, the LNOI wafer can be made
169   larger without much difficulty [33].

170

171   **Figure 4.** (**a**) Transmission spectrum of the LN microring resonator. (**b**) The Lorentz fitting (red
172   curve) reveals a loaded Q factor of 5.70×10^6, corresponding to an intrinsic Q factor of $1.14 \times
173   10^7$. Inset: The optical mode distribution and n_{eff} in the ring waveguide calculated using FDTD
174   simulation.

175   The optical loss characterization was performed using whispering-gallery-resonator-loss
176   measurements. The propagation loss α is related to Q-factor of the ring resonator as mentioned

177   before. Figure 4a shows the measured transmission spectrum for the wavelength range
178   between 1546 nm and 1564 nm. The free spectral range (FSR) of the microring resonator is
179   determined to be 2.71 nm, which is consistent with the diameter of our ring resonator of 160
180   μm. The resonant lines appear regularly spaced, indicating that mostly only the low-order
181   modes exist in the ring resonator. One of the whispering-gallery modes at the resonant
182   wavelength of 1560.48 nm is chosen for the measurement of the loaded Q-factor by fitting with
183   a Lorentz function, which reached 5.07×10^6, corresponding to an intrinsic Q-factor of $1.14 \times$
184   10^7 in the critical coupling regime as evidenced by Figure 4b. The effective refractive index n_{eff}
185     $= \lambda^2 / (2\pi R \cdot FSR)$, with the ring radius of R = 80 μm and wavelength of 1560.48 nm, is calculated
186   to be 1.79, which is in good agreement with our FDTD simulation result given in the inset of
187   Figure 4b. Combining the effective refractive index and the Q-factor obtained from the
188   transmission spectrum, the propagation loss in the microring resonator is calculated to be 0.027
189   dB/cm using the aforementioned expression $\alpha = 2\pi n_{eff} / (Q\lambda)$. This result represents the upper
190   limit of the propagation loss in the LNOI waveguide fabricated using our method.

191   **4. Discussion**

192   The low propagation loss of 0.027 dB/cm is a result of the low surface roughness of
193   R_q=0.452 nm on the fabricated LNOI waveguides. This is benefitted from our technique in
194   which the LNOI is purely patterned by the chemo-mechanical polishing without any use of the
195   ion beam etching [30]. The ion beam etching inherently leaves a small amount of surface
196   roughness on the nearly vertical sidewalls which is difficult to be completely removed by top
197   surface polishing [34,35]. This is the major reason that we are able to obtain a propagation loss
198   lower than the waveguides fabricated by FIB or reactive ion etching. In the current experiment,
199   we used a femtosecond laser to pattern the Cr hard mask. Generally speaking, the sidewall
200   roughness on the Cr mask patterned by the femtosecond laser ablation should be higher than
201   the surface roughness on the LNOI photonic structures produced with the ion beam etching.
202   However, the sidewall roughness on the Cr mask will only be transferred to the underneath
203   LNOI near the top surface, thus it can be completely suppressed with an additional polishing
204   process for thinning the LNOI substrate after the removal of the Cr mask (see, Figure 1d).
205   It should be mentioned that the propagation loss obtained by measuring the Q factor of
206   the ring resonator may have been underestimated for the straight segments in the LNOI
207   waveguides as presented in Figure 3d - f due to a higher radiative loss in the ring resonator.
208   Ultimately, the propagation loss in the LNOI waveguides is limited by the absorption in
209   crystalline LN which is well known to be on the order of $\sim 10^{-3}$ dB/cm. Our measured loss is still
210   one order of magnitude away from the theoretical limit, which could be attribute to several
211   likely factors including the radiative loss in the ring resonator, some unknown contamination
212   on the surface of LNOI waveguide as the measurements are all carried out in a low-class clean
213   room, existence of absorptive defects in the LNOI substrate owing to the imperfect crystal
214   growth, and the remaining surface roughness left by the chemo-mechanical polishing process.
215   Thus, to realize LNOI waveguides with propagation losses on the order of 10^{-3} dB/cm, a lot of
216   refinements should be systematically investigated in the future.
217   The fabrication resolution of femtosecond laser direct writing is typically on the order of
218   1 μm for inorganic materials such as glass, semiconductor and metal. However, today's optical
219   lithography can easily achieve sub-micron or even 100 nm-level patterning resolutions. This
220   should be sufficient for fabricating single mode LNOI waveguides of narrower widths by
221   which PICs such as Mach-Zender interferometers and polarization convertors can be built.
222   Moreover, the mode field of the LNOI waveguides can be tuned by coating them with fused
223   silica for suppressing higher order modes as well as scattering loss thanks to the reduced
224   contrast of the refractive index between the LNOI waveguide and the cladding environment
225   [36]. With all of these improvements, the LNOI waveguides will become a major building block
226   for PIC applications.

5. Conclusions

To conclude, we have achieved a propagation loss of 0.027 dB/cm in LNOI waveguides fabricated by a combination of femtosecond laser micromachining for patterning the Cr mask and chemo-mechanical polishing for transferring the laser-written patterns to the LNOI beneath the Cr mask. By eliminating the low-throughput FIB or EBW process, our technique can enable rapid fabrication of low-loss optical waveguides of great lengths which are only limited by the motion range of the air bearing stage and the size of LNOI wafers. Thus, our approach greatly promotes the fabrication efficiency and reduces the cost in the manufacturing of LNOI PICs. The waveguides as well as ring resonators can be adopted for constructing complex PICs, opening the avenue for mass production of LNOI PICs for optical communication and computation applications.

References

1. Ladd, T.D.; Jelezko, F.; Laflamme, R.; Nakamura, Y.; Monroe, C.; O'Brien, J.L. Quantum computers. *Nature* **2010**, *464*, 45, doi:10.1038/nature08812.

2. Shen, Y.; Harris, N.C.; Skirlo, S.; Prabhu, M.; Baehr-Jones, T.; Hochberg, M.; Sun, X.; Zhao, S.; Larochelle, H.; Englund, D., et al. Deep learning with coherent nanophotonic circuits. *Nature Photon.* **2017**, *11*, 441, doi:10.1038/nphoton.2017.93.

3. Harris Nicholas, C.; Bunandar, D.; Pant, M.; Steinbrecher Greg, R.; Mower, J.; Prabhu, M.; Baehr-Jones, T.; Hochberg, M.; Englund, D. Large-scale quantum photonic circuits in silicon. In *Nanophotonics*, 2016; Vol. 5, p 456, doi:10.1515/nanoph-2015-0146.

4. Dietrich, C.P.; Fiore, A.; Thompson, M.G.; Kamp, M.; Höfling, S. GaAs integrated quantum photonics: Towards compact and multi-functional quantum photonic integrated circuits. *Laser Photon. Rev.* **2016**, *10*, 870-894, doi:10.1002/lpor.201500321.

5. Najafi, F.; Mower, J.; Harris, N.C.; Bellei, F.; Dane, A.; Lee, C.; Hu, X.; Kharel, P.; Marsili, F.; Assefa, S., et al. On-chip detection of non-classical light by scalable integration of single-photon detectors. *Nature Comm.* **2015**, *6*, 5873, doi:10.1038/ncomms6873

6. Yang, K.Y.; Oh, D.Y.; Lee, S.H.; Yang, Q.-F.; Yi, X.; Shen, B.; Wang, H.; Vahala, K. Bridging ultrahigh-Q devices and photonic circuits. *Nature Photon.* **2018**, *12*, 297-302, doi:10.1038/s41566-018-0132-5.

7. Qiang, X.; Zhou, X.; Wang, J.; Wilkes, C.M.; Loke, T.; O'Gara, S.; Kling, L.; Marshall, G.D.; Santagati, R.; Ralph, T.C., et al. Large-scale silicon quantum photonics implementing arbitrary two-qubit processing. *Nature Photon.* **2018**, *12*, 534-539, doi:10.1038/s41566-018-0236-y.

8. Marshall, G.D.; Politi, A.; Matthews, J.C.F.; Dekker, P.; Ams, M.; Withford, M.J.; O'Brien, J.L. Laser written waveguide photonic quantum circuits. *Opt. Express* **2009**, *17*, 12546-12554, doi: 10.1364/OE.17.012546.

9.   Sohler, W.; Hu, H.; Ricken, R.; Quiring, V.; Vannahme, C.; Herrmann, H.; Büchter, D.; Reza, S.; Grundkötter, W.; Orlov, S., et al. Integrated optical devices in lithium niobate. *Opt. Photon. News* **2008**, *19*, 24-31, doi:10.1364/OPN.19.1.000024.

10. Jin, H.; Liu, F.M.; Xu, P.; Xia, J.L.; Zhong, M.L.; Yuan, Y.; Zhou, J.W.; Gong, Y.X.; Wang, W.; Zhu, S.N. On-chip generation and manipulation of entangled photons based on reconfigurable lithium-niobate waveguide circuits. *Phys. Rev. Lett.* **2014**, *113*, 103601, doi:10.1103/PhysRevLett.113.103601.

11. Lin, J.; Xu, Y.; Fang, Z.; Song, J.; Wang, N.; Qiao, L.; Fang, W.; Cheng, Y. Second harmonic generation in a high-Q lithium niobate microresonator fabricated by femtosecond laser micromachining. *arXiv preprint arXiv:1405.6473* **2014**.

12. Wang, J.; Bo, F.; Wan, S.; Li, W.; Gao, F.; Li, J.; Zhang, G.; Xu, J. High-Q lithium niobate microdisk resonators on a chip for efficient electro-optic modulation. *Opt. Express* **2015**, *23*, 23072-23078, doi: 10.1364/OE.23.023072.

13. Wang, C.; Burek, M.J.; Lin, Z.; Atikian, H.A.; Venkataraman, V.; Huang, I.-C.; Stark, P.; Lončar, M. Integrated high quality factor lithium niobate microdisk resonators. *Opt. Express* **2014**, *22*, 30924-30933, doi: 10.1364/OE.22.030924.

14. Lin, J.; Xu, Y.; Fang, Z.; Wang, M.; Song, J.; Wang, N.; Qiao, L.; Fang, W.; Cheng, Y. Fabrication of high-Q lithium niobate microresonators using femtosecond laser micromachining. *Sci. Rep.* **2015**, *5*, 8072, doi: 10.1038/srep08072.

15. Lin, J.; Xu, Y.; Ni, J.; Wang, M.; Fang, Z.; Qiao, L.; Fang, W.; Cheng, Y. Phase-matched second-harmonic generation in an on-chip LiNbO$_3$ microresonator. *Phys. Rev. Appl.* **2016**, *6*, 014002, doi: 10.1103/PhysRevApplied.6.014002.

16. Lin, J.; Xu, Y.; Fang, Z.; Wang, M.; Wang, N.; Qiao, L.; Fang, W.; Cheng, Y. Second harmonic generation in a high-Q lithium niobate microresonator fabricated by femtosecond laser micromachining. *Sci. China Phys. Mech. Astron.* **2015**, *58*, 114209, doi: 10.1007/s11433-015-5728-x.

17. Hao, Z.; Wang, J.; Ma, S.; Mao, W.; Bo, F.; Gao, F.; Zhang, G.; Xu, J. Sum-frequency generation in on-chip lithium niobate microdisk resonators. *Photon. Res.* **2017**, *5*, 623-628, doi: 10.1364/PRJ.5.000623.

18. Wang, L.; Wang, C.; Wang, J.; Bo, F.; Zhang, M.; Gong, Q.; Lončar, M.; Xiao, Y.-F. High-Q chaotic lithium niobate microdisk cavity. *Optics Lett* **2018**, *43*, 2917-2920, doi:10.1364/OL.43.002917.

19. Luo, R.; Jiang, H.; Rogers, S.; Liang, H.; He, Y.; Lin, Q. On-chip second-harmonic generation and broadband parametric down-conversion in a lithium niobate microresonator. *Opt. Express* **2017**, *25*, 24531-24539, doi: 10.1364/OE.25.024531.

20. Jiang, W.C.; Lin, Q. Chip-scale cavity optomechanics in lithium niobate. *Sci. Rep.* **2016**, *6*, 36920, doi: 10.1038/srep36920.

21. Fang, Z.; Xu, Y.; Wang, M.; Qiao, L.; Lin, J.; Fang, W.; Cheng, Y. Monolithic integration of a lithium niobate microresonator with a free-standing waveguide using femtosecond laser assisted ion beam writing. *Sci. Rep.* **2017**, *7*, 45610, doi: 10.1038/srep45610.

22. Liang, H.; Luo, R.; He, Y.; Jiang, H.; Lin, Q. High-quality lithium niobate photonic crystal nanocavities. *Optica* **2017**, *4*, 1251-1258, doi:10.1364/OPTICA.4.001251.

23. Wang, C.; Zhang, M.; Stern, B.; Lipson, M.; Lončar, M. Nanophotonic lithium niobate electro-optic modulators. *Opt. Express* **2018**, *26*, 1547-1555, doi: 10.1364/OE.26.001547.

24. Wang, C.; Xiong, X.; Andrade, N.; Venkataraman, V.; Ren, X.-F.; Guo, G.-C.; Lončar, M. Second harmonic generation in nano-structured thin-film lithium niobate waveguides. *Opt. Express* **2017**, *25*, 6963-6973, doi:10.1364/OE.25.006963.

25. Luo, R.; He, Y.; Liang, H.; Li, M.; Lin, Q. Highly tunable efficient second-harmonic generation in a lithium niobate nanophotonic waveguide. *Optica* **2018**, *5*, 1006-1011, doi:10.1364/OPTICA.5.001006.

26. Cai, L.; Han, H.; Zhang, S.; Hu, H.; Wang, K. Photonic crystal slab fabricated on the platform of lithium niobate-on-insulator. *Optics Lett* **2014**, *39*, 2094-2096, doi:10.1364/OL.39.002094.

27. Diziain, S.; Geiss, R.; Steinert, M.; Schmidt, C.; Chang, W.-K.; Fasold, S.; Füßel, D.; Chen, Y.-H.; Pertsch, T. Self-suspended micro-resonators patterned in Z-cut lithium niobate membranes. *Opt. Mater. Express* **2015**, *5*, 2081-2089, doi:10.1364/OME.5.002081.

28. Krasnokutska, I.; Tambasco, J.-L.J.; Li, X.; Peruzzo, A. Ultra-low loss photonic circuits in lithium niobate on insulator. *Opt. Express* **2018**, *26*, 897-904, doi:10.1364/OE.26.000897.

328   29.   Wolf, R.; Breunig, I.; Zappe, H.; Buse, K. Scattering-loss reduction of ridge waveguides by sidewall
329   polishing. *Opt. Express* **2018**, *26*, 19815-19820, doi:10.1364/OE.26.019815.
330   30.   Wu, R.; Zhang, J.; Yao, N.; Fang, W.; Qiao, L.; Chai, Z.; Lin, J.; Cheng, Y. Lithium niobate micro-disk
331   resonators of quality factors above 10^7. *Optics Lett* **2018**, *43*, 4116-4119, doi:10.1364/OL.43.004116.
332   31.   Poberaj, G.; Hu, H.; Sohler, W.; Guenter, P. Lithium niobate on insulator (LNOI) for micro-photonic
333   devices. *Laser Photon. Rev.* **2012**, *6*, 488-503, doi: 10.1002/lpor.201100035.
334   32.   Sugioka, K.; Cheng, Y. Ultrafast lasers—reliable tools for advanced materials processing. *Light Sci.*
335   *Appl.* **2014**, 3, e149, doi: 10.1038/lsa.2014.30.
336   33.   Boes, A.; Corcoran, B.; Chang, L.; Bowers, J.; Mitchell, A. Status and potential of lithium niobate on
337   insulator (LNOI) for photonic integrated circuits. *Laser Photon. Rev.* **2018**, 12, 1700256, doi:
338   10.1002/lpor.201700256.
339   34.   Wolf, R.; Breunig, I.; Zappe, H.; Buse, K. Cascaded second-order optical nonlinearities in on-chip
340   micro rings. *Opt. Express* **2017**, *25*, 29927-29933, doi:10.1364/OE.25.029927.
341   35.   Wolf, R.; Breunig, I.; Zappe, H.; Buse, K. Q-factor enhancement of integrated lithium-niobate-on-
342   insulator ridge waveguide whispering-gallery-mode resonators by surface polishing. In
343   Proceedings of Laser Resonators, Microresonators, and Beam Control XIX; **2017**, p. 1009002, doi:
344   10.1117/12.2251516.
345   36.   Guarino1, A.; Poberaj, G.; Rezzonico, D.; Degl'Innocenti, R.; Günter, P. Electro–optically tunable
346   microring   resonators   in   lithium   niobate.   *Nature   Photon.*   **2007**,   *1*,   407-410,
347   doi:10.1038/nphoton.2007.93.